Theoretical Assessment of the Structure and Stability of the λ Phase of Nitrogen

Watit Sontising[1] and Gregory J. O. Beran[1,*]

[1]*Department of Chemistry, University of California, Riverside, California 92521 USA*

The λ phase of nitrogen was reported in 2016 and is one of more than a dozen high-pressure solid nitrogen forms that have been discovered. However, its crystal structure could not be solved unambiguously from powder diffraction alone; rather the reported structure was determined by combining experimental monoclinic lattice parameters with atomic positions from an earlier, computationally predicted structure that had similar unit cell dimensions. Here, we revisit this structure using density functional theory and higher-level fragment-based second-order Møller-Plesset perturbation theory (MP2) and coupled cluster singles, doubles, and perturbative triples (CCSD(T)). Crystal structure prediction is performed to demonstrate that the reported $P2_1/c$ structure is indeed the likeliest candidate for the λ phase. Furthermore, we provide further evidence for the structural assignment by demonstrating good agreement between its predicted and experimental structural parameters and Raman spectra. Finally, the thermodynamic stability of the λ phase relative to other phases has been uncertain, but the calculations do suggest that it may be the thermodynamically most stable phase for at least part of the pressure range over which it has been observed.

I. INTRODUCTION

Solid nitrogen exhibits fascinating phase behavior at high pressures, with at least 13 molecular and polymeric phases reported.[1] Some of these phases exhibit well-defined regions of thermodynamic stability. Others are kinetically accessible but thermodynamically metastable polymorphs, as evidenced by the often overlapping temperature and pressure conditions reported for different phases. These factors make mapping out the phase diagram (Figure 1) challenging. Furthermore, solving the crystal structure for high-pressure phases can also be difficult. The structures for the ζ,[2–5] θ,[6] and κ phases[5] are currently unknown, for example. The structure of the ι phase was reported only in 2018.[7]

The monoclinic λ phase was discovered in 2016.[1] This molecular nitrogen phase can be synthesized by compression of high-purity liquid nitrogen at low temperatures. It has been stabilized between 0.3-110 GPa at 77 K and between 32-140 GPa at 300 K. Like the ζ-phase, λ nitrogen transforms into the η phase at pressures above 100 GPa. This exceptionally wide range of pressure stability means that the λ phase can coexist with nine other phases: the γ, ϵ, ζ, ι, θ, κ, amorphous η, polymeric *cg*, and polymeric layered phases. It remains unclear whether the λ phase is thermodynamically preferred or only metastable relative to these other phases in this region of the phase diagram.

Solving the crystal structure of λ nitrogen experimentally proved challenging. Full Rietveld refinement of the structure from powder X-ray diffraction data was not possible due to the small sample sizes, sample graininess, and low X-ray scattering intensities for nitrogen.[1] Instead, the crystal structure determination relied heavily on an earlier density functional theory (DFT) crystal structure prediction study.[8] That study identified several low-enthalpy monoclinic and orthorhombic crystal structures which had not previously been observed experimentally. Frost and co-workers[1] found that fitting their experimental diffraction data to a monoclinic cell produced lattice parameters in fairly good agreement with the previously predicted $P2_1/c$ structure. Their final reported crystal structure was then constructed by combining the experimental lattice parameters with the previously predicted fractional coordinates of the atoms.

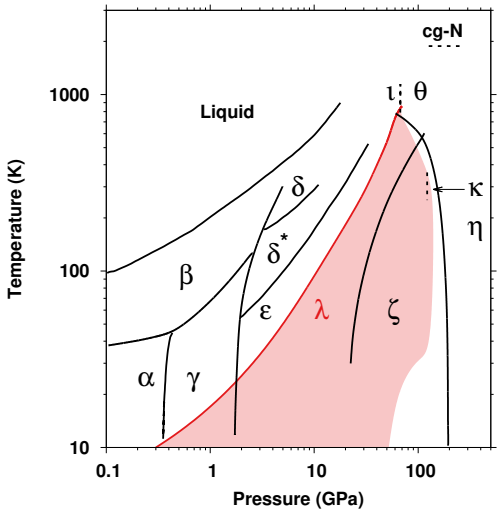

FIG. 1: Phase diagram of nitrogen. The λ phase has been observed over the conditions highlighted in red, though its thermodynamic stability relative to the other phases remains unclear.

While this structural determination approach is reasonable, further evidence for the determined structure would be beneficial. For example, the long-accepted structure of phase III carbon dioxide, which was solved from relatively challenging powder x-ray diffraction data,[9] has recently been challenged. High-quality mod-

eling and comparison against a variety of experimental data found in the literature suggest that carbon dioxide phases III and VII are actually identical, with phase VII being the true structure.[10] Density functional theory predictions of the structures and Raman spectrum were used to help confirm the ι structure as well.[7]

Here, we re-visit the λ phase of nitrogen computationally to provide further structural and spectroscopic evidence for the reported crystal structure and to assess its overall thermodynamic stability. Modeling molecular nitrogen in the solid state can be difficult. The weak, non-specific non-covalent interactions between molecules produce a relatively flat crystal energy landscape, with many possible crystal structures exhibiting similar energetic stabilities. For example, the 2009 DFT crystal structure prediction study[8] whose results were used to help solve the λ N_2 structure found several low-enthalpy structures within ∼0.5 kJ/mol of each other at 40 GPa.

When discriminating between such closely ranked crystal structures, it is important to model the interactions carefully. The neglect of van der Waals dispersion interactions in the 2009 DFT study could impact the relative energies, for example. Further insights and energy refinement can be gained by employing higher-level correlated wave function techniques such as second-order Møller-Plesset perturbation theory (MP2) or even coupled cluster models. Periodic local MP2 calculations have provided insight into the phase transitions between the α, γ, ϵ, and polymeric *cg* phases,[11,12] but such calculations are relatively expensive, and nuclear gradients that would allow geometry optimizations and other response properties to be predicted readily have not been implemented.

Alternatively, fragment-based methods[13–16] such as the hybrid many-body interaction (HMBI) model[17–19] provide an computationally practical strategy for applying high-level correlated wave function methods to periodic systems. In HMBI, individual molecules and their short-range pairwise intermolecular interactions are modeled with MP2 or other high-level electronic structure methods, while longer-range pairwise interactions and non-additive many-body intermolecular interactions arising from the infinite lattice are approximated with a polarizable force field. When coupled with a quasi-harmonic treatment of thermal expansion, the HMBI model predicts structural, mechanical, and spectroscopic properties of several phases of carbon dioxide in excellent agreement with experiment.[10,20–22] HMBI-predicted structural and spectroscopic data was used to support the aforementioned argument that carbon dioxide phases III and VII are the same phase.[10] The HMBI fragment approach also predicts the polymorphic phase diagram of methanol with ∼0.5 kJ/mol accuracy,[23,24] and it has been applied to larger polymorphic organic crystals such as aspirin[25] and oxalyl dihydrazide.[26] The related binary interaction fragment model[27,28] has proved similarly effective for modeling molecular crystal structures and properties in solid hydrogen fluoride,[29,30] carbon dioxide,[31–34] and ices.[35–37]

Here, we investigate the λ phase of nitrogen using a mixture of periodic planewave DFT theory and fragment-based MP2 calculations. We confirm the previously reported structure of the λ phase through a combination of DFT-based crystal structure prediction (employing *ab initio* random structure searching, or AIRSS) and higher-level refinement with MP2. Further support for the λ phase structure is provided by comparison between the predicted and experimentally observed Raman spectra. Finally, to investigate whether the λ phase is a thermodynamically stable phase on the phase diagram (rather than a kinetically accessible metastable one), the thermodynamic stability of the λ phase relative to several other experimentally known phases which can exist under the same thermodynamic conditions is investigated.

II. METHODS

Density functional theory calculations: DFT calculations were employed to optimize structures and provide an initial stability ranking. The calculations were performed using the B86bPBE density functional[38,39] with the exchange-hole dipole moment (XDM) dispersion correction,[40] an 80 Ry planewave cutoff, and a 6×6×6 Monkhorst-Pack k-point grid, as implemented in Quantum Espresso version 6.2.1.[41,42] Projector-augmented wave (PAW) potentials for nitrogen atoms were produced using A. Dal Corso's Atomic code v6.1. External pressure was applied to the variable cell optimizations to mimic the experimental conditions. See Supplemental Information for validation and convergence testing of the DFT models.

Fragment-based hybrid many-body interaction (HMBI) calculations: The structures and stability rankings of the DFT structures were subsequently refined with correlated wave function methods via the HMBI model.[17–19] HMBI decomposes the total energy of the crystal according to a many-body expansion,

$$\begin{aligned} E^{HMBI}_{crystal} &= E^{QM}_{\text{1-body}} + E^{QM}_{SR\ \text{2-body}} + E^{MM}_{LR\ \text{2-body}} \\ &\quad + E^{MM}_{\text{many-body}} \end{aligned} \tag{1}$$

where 1-body terms correspond to the energies of individual nitrogen molecules in the unit cell, two-body terms to the interaction energies between pairs of molecules (both within the central unit cell and involving periodic image molecules), and many-body terms to the non-additive three-body and higher contributions. The 1-body and short-ranged two-body terms (i.e. dimers separated by no more than 6 Å) were computed with MP2 or CCSD(T), while the long-range two-body and many-body terms are approximated using the periodic Hartree-Fock (pHF) or AMOEBA polarizable force field[43]c calculations under periodic boundary conditions. The number of monomer and dimer fragments that need to be computed is reduced by exploiting space group symmetry.[44]

The density-fitted MP2 calculations were performed using Molpro 2012,[45] CCSD(T) calculations (with

core electrons frozen) were employed using PSI4 v1.0,[46] the pHF calculations were carried out using CRYSTAL17,[47] and the polarizable force field calculations were conducted using the Tinker version 6.3.[48] Existing AMOEBA force field parameters were used for the N_2 molecule.[43] Single-point MP2 and CCSD(T) fragment energies were computed with counterpoise correction at the extrapolated complete basis set (CBS) limit. The CBS results were estimated via the combination of HF/aug-cc-pVQZ energies plus two-point extrapolation of the correlation energy contributions[49] obtained from the aug-cc-pVTZ and aug-cc-pVQZ basis sets. The impact of basis set on predicted energies in small molecule crystals has been studied extensively elsewhere.[16,21,22] Single-point pHF fragment energies were computed using the pob-TZVP basis set,[50] which is version of the popular def2-TZVP basis set[51] that has been adapted for periodic calculations. Empirical testing in small nitrogen clusters suggests that this basis set, with no counterpoise correction, provides intermolecular many-body HF interaction energies that agree fairly well with those obtained from much larger basis sets.

Structure refinement and quasi-harmonic approximation: Because the predicted molar volume is sensitive to the level of theory and because the HMBI-based MP2 or CCSD(T) calculations can potentially provide higher-accuracy structures than those from the DFT model, one would like to refine the structures at the MP2/CCSD(T) levels of theory. Full crystal relaxations with MP2 or CCSD(T) are somewhat more computationally expensive than those with DFT (especially with the larger basis sets needed for the correlated wave function models). To make the initial structure refinements less expensive, the following simplified quasi-1-D optimization approach was employed: First, the geometries were optimized with DFT at a series of external pressures. Second, single-point HMBI electronic energies were computed with MP2 or CCSD(T) and different many-body treatments at each DFT geometry. A PV pressure-volume contribution was added to the resulting energies to obtain enthalpies versus volume: $H = E(V) + PV$. The enthalpy-volume curves were fitted to the Murnaghan equation of state,

$$H(V) = H_0 + \frac{B_0 V}{B_0^{'}}\left[\frac{(V_0/V)^{B_0^{'}}}{B_0^{'}-1}+1\right] - \frac{B_0 V_0}{B_0^{'}-1} \quad (2)$$

where the enthalpy (H_0), volume (V_0), bulk modulus (B_0), and its first pressure derivative ($B_0^{'}$) at zero pressure are the fitting parameters. The optimal volume V_0 and corresponding enthalpy H_0 were extracted from the minimum of the fit. Atomic coordinates were obtained via interpolation of the DFT fractional coordinates to the optimal volume extracted from the equation of state fit. This approach is similar to how the quasi-harmonic approximation (QHA) is sometimes performed (see Ref 22, for example), except the zero-point and thermal vibrational contributions are neglected here. This neglect is reasonable at higher pressures where thermal expansion effects are expected to be small.

For the most promising λ phase structure candidate, full QHA calculations including phonon contributions were performed. DFT geometry optimizations were carried out over a wide pressure range (at 28 pressures ranging 0–150 GPa). Again, MP2 and CCSD(T) single-point energy refinements were computed using HMBI, as described above. Harmonic Γ-point phonons were computed at the DFT level, and the volume-dependence of the phonon frequencies was approximated using mode-specific Grüneisen parameters that were computed via finite-difference, as described previously.[22] Optimal volumes and energies were then obtained by minimizing the Gibbs free energies,

$$G(T,P) = E(V) + PV + F_{vib}(T) \quad (3)$$

where F_{vib} is the standard harmonic Helmholtz vibrational free energy. This combination of DFT geometries and phonons plus higher-level energies in quasi-harmonic calculations effectively reproduced thermal expansion and thermochemical properties in an earlier study on several small-molecule crystals.[22]

Simulated powder X-ray diffraction (PXRD) and Raman spectra: PXRD and Raman spectra were modeled at the HMBI MP2 level for comparison with experiment. To do so, the crystal structure was relaxed at the HMBI MP2/aug-cc-pVDZ + AMOEBA level using fixed unit cell parameters determined from the HMBI MP2/CBS QHA calculations described above. Previous work on carbon dioxide[10] demonstrated that when the unit cell is constrained with the lattice parameters obtained from a high level of theory, relaxing the atomic positions and predicting spectroscopic properties with MP2 in a smaller basis set does not introduce substantial errors compared to larger basis set results, since the unit cell dimensions constrain the packing density.

Simulated PXRD spectra were generated using Mercury[52] and the same 0.42418 Å wavelength as the experiments. Simulated Raman spectrum are based on Γ-point MP2/aug-cc-pVDZ + AMOEBA harmonic phonon frequencies, using the analytical Hessian algorithms implemented in Gaussian 09.[53] The use of analytical Hessians for each fragment contribution helps reduce numerical artifacts associated with summing contributions from many fragment Hessians in the HMBI model. Raman intensities were calculated from finite difference of polarizability derivatives, which were approximated via the QM 1- and 2-body contributions only (no AMOEBA or periodic HF many-body contribution). Because intermolecular many-body contributions are relatively small in nitrogen, the effect on the Raman intensities from neglecting the many-body contributions to the polarizability derivatives should be small. This approach has been described previously.[10,35] Peaks in the simulated Raman spectra are plotted with an arbitrary full width at half maximum of 10 cm^{-1}.

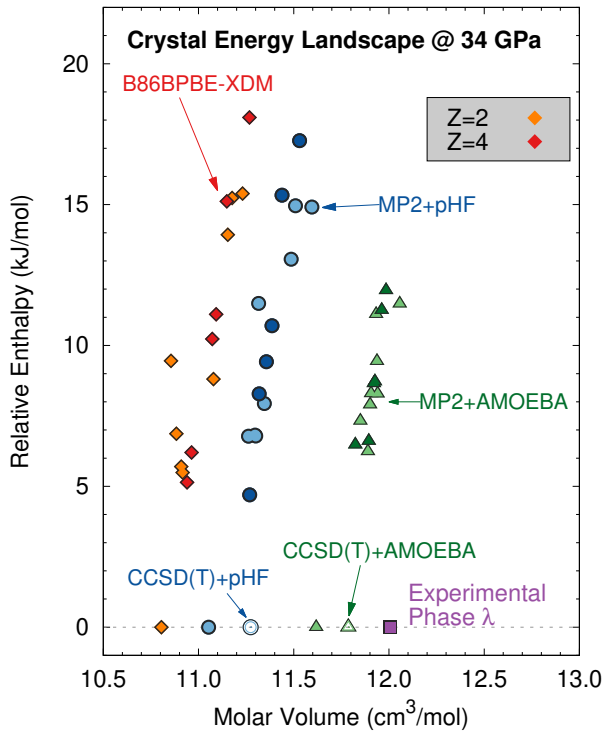

FIG. 2: Crystal energy landscape for the low-energy crystal structures at 34 GPa with the B86bPBE-XDM (red Z=4/orange Z=2), MP2/CBS + pHF (dark blue Z=4/light blue Z=2), and MP2/CBS + AMOEBA (dark green Z=4/light green Z=2) levels of theory. Open symbols correspond to further CCSD(T) refinements of the structures. The experimentally inferred molar volume is indicated in purple. Enthalpies at each level of theory are plotted relative to the lowest-energy structure.

III. RESULTS AND DISCUSSION

Crystal structure prediction: To explore the landscape of potential crystal structures, crystal structure prediction was performed via *ab initio* random structure searching (AIRSS).[54] Employing experimental constraints can facilitate AIRSS by narrowing the search space, as demonstrated for the unusually complex structure of ι N_2.[7] Experimental reports indicate that the λ N_2 phase adopts monoclinic space group symmetry with two molecules in the unit cell (Z=2).[1] Accordingly, the AIRSS search was performed over all 13 monoclinic space groups with Z=2. Structures were generated by placing a single nitrogen molecule at one possible Wyckoff position with random orientation and then applying the space group symmetry operators to populate the other molecules in the unit cell. Lattice parameters were randomized within the constraint that the unit cell volume remained within ±40% of the experimentally reported value of 39.9 Å^3 (or 12.0 cm^3/mol) at 34 GPa. Because the $C2$, Cm, Cc, and $C2/c$ space groups are not amenable to Z=2, searches in those groups were run with Z=4. The Z=4 searches produced a mixture of new structures and structures which were supercell representations of previously predicted Z=2 structures.

In the end, at least 100 random structures were generated for each space group, for a total of over 1,300 structures. Each structure was fully relaxed with B86bPBE-XDM at 34 GPa of external pressure. Some of the random structures adopted covalent/polymeric forms upon relaxation. At 34 GPa, the DFT enthalpies of the polymeric structures are significantly higher than those of molecular forms, so they were discarded. In the end, the AIRSS procedure generated 636 molecular structures with Z=2 and 246 with Z=4. After clustering to remove duplicate structures, 22 unique structures remained.

Figure 2 compares the crystal energy structure for the 15 structures whose B86bPBE-XDM energies lie within 20 kJ/mol of the most stable structure. Higher-energy structures are unlikely to occur experimentally, since the typical energy window for polymorphism is ∼10 kJ/mol.[55,56] Pictures, lattice parameters, atomic coordinates, and energetics for these predicted structures are provided in the Supplemental Information. All of the DFT-predicted structures exhibit molar volumes ranging 10.8–11.3 cm^3/mol, which is 6–10% smaller than the 12.0 cm^3/mol inferred from the diffraction experiments.[1] The neglect of expansion arising from zero-point energy and thermal vibrational contributions will likely cause some volume underestimation, but those effects should be small at 34 GPa. Large volume errors are potentially problematic when comparing different nitrogen phases, since many nitrogen phase changes at high-pressure occur with volume changes of as little as 2%.

Refinement of the structures with correlated fragment-based MP2/CBS with either pHF or AMOEBA many-body treatments alters the relative enthalpies of the different candidate structures, but all models predict the same densely packed $P2_1/c$ structure to be the most stable one. This structure is identical to the $P2_1/c$ structure predicted by Pickard and Needs[8] and which has been ascribed to the λ phase.[1] Though the relative enthalpies differ depending on the model, all models predict that this structure is more stable than the second-lowest structure by ∼5 kJ/mol or more.

MP2 + pHF and MP2 + AMOEBA refinement also increase the molar volumes by ∼2% and ∼9%, on average, to 11.1–11.6 and 11.6–12.1 cm^3/mol, respectively (Figure 2). With both many-body treatments, the volume of the lowest-energy structure shifts closer toward the experimental value of 12.0 cm^3/mol. Switching from MP2 to CCSD(T) increases the molar volumes further, by about 0.2 cm^3/mol. At the CCSD(T)/CBS + AMOEBA level, the molar volume of 11.8 cm^3/mol is 2% smaller than the experimentally reported one.

These results demonstrate some sensitivity of the predictions to the many-body treatment. With the monomer and dimer contributions in the fragment model treated with large-basis MP2 or CCSD(T), the largest re-

TABLE I: Comparison of experimental and predicted lattice parameters for λ N_2 at 34 GPa.

	a (Å)	b (Å)	c (Å)	β (°)	Volume (cm^3/mol)
B86bPBE-XDM	2.951	2.916	5.638	132.32	10.80
MP2/CBS + pHF	2.975	2.945	5.663	132.71	11.05
QHA MP2/CBS + pHF (300 K)	2.985	2.957	5.674	132.26	11.16
QHA CCSD(T)/CBS + pHF (300 K)	3.005	2.979	5.701	132.20	11.38
QHA MP2/CBS + AMOEBA (300 K)	3.035	3.010	5.750	132.09	11.74
QHA CCSD(T)/CBS + AMOEBA (300 K)	3.046	3.023	5.768	132.05	11.87
Experiment (300 K)[1]	3.051(7)	3.066(5)	5.705(13)	131.65(5)	12.01

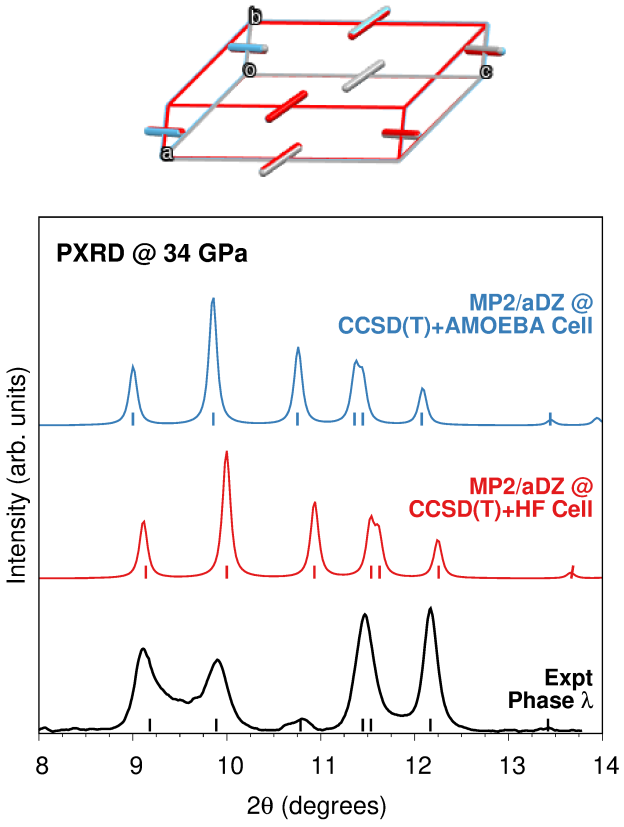

FIG. 3: Structure overlay (top) and simulated powder x-ray diffraction spectrum (bottom) comparing the experimental,[1] CCSD(T)/CBS + periodic HF, and CCSD(T)/CBS + AMOEBA crystal structures.

maining source of error probably lies in the more approximate many-body treatment. One would typically expect the quantum mechanical pHF treatment to perform better than the AMOEBA one, as has been observed in other small-molecule crystals.[22,23] At high pressures, the HF many-body exchange-overlap description should be superior to that of the simplified short-range polarization damping model employed AMOEBA force field (and which was parameterized at ambient conditions). For this nitrogen phase, however, the AMOEBA many-body treatment predicts volumes closer to experiment at 34 GPa. As will be discussed below, however, the periodic HF many-body treatment does predict molar volume in closer agreement with experiment at higher pressures. Interestingly, the range of relative enthalpies for the higher-lying structures is considerably smaller with the MP2 + AMOEBA model than for the MP2 + pHF or DFT models. In the end, results from both many-body treatments are presented throughout the remainder of the paper to help quantify the uncertainties in the predictions with respect to the treatment of the many-body interactions.

As noted above, the slight underestimation of the molar volumes here is consistent with the neglect of zero-point and thermal vibrational contributions. Quasi-harmonic calculations that estimate these contributions were performed on this most-stable structure. Table I compares the lattice parameters predicted from several different models against experiment. As expected given the high pressure, thermal expansion effects are small, increasing individual lattice constants by ∼0.01 Å and the total molar volume by only ∼0.1 cm^3/mol. Earlier work on phase I carbon dioxide found that expansion effects due to vibrational contributions were most significant below ∼10–20 GPa.[20] To enable the prediction of additional properties, the atomic positions here obtained from the initial DFT optimizations were relaxed at the MP2/aug-cc-pVDZ + AMOEBA level of theory, holding the lattice parameters fixed at their predicted QHA CCSD(T)/CBS values.

With either many-body treatment, the final QHA CCSD(T) predictions at 300 K and 34 GPa reproduce the experimental lattice constants within 0.06 Å and 0.4°, and in the case of the QHA CCSD(T) + AMOEBA, reproduce the volume to to within ∼0.1 cm^3/mol. The rmsd15,[57] which measures of the root-mean-square deviations for a 15-molecule cluster taken from the crystal, is an excellent 0.037 Å between this structure and the experimental one. Overlays of the predicted and experimental structures are shown in Figure 3. Similarly, the simulated PXRD patterns predicted from these CCSD(T) structures reproduce the experimental peak positions fairly well, especially for the CCSD(T)/CBS + AMOEBA cell whose lattice constants are in best agreement with those reported experimentally. The combination of good agreement between the predicted and ex-

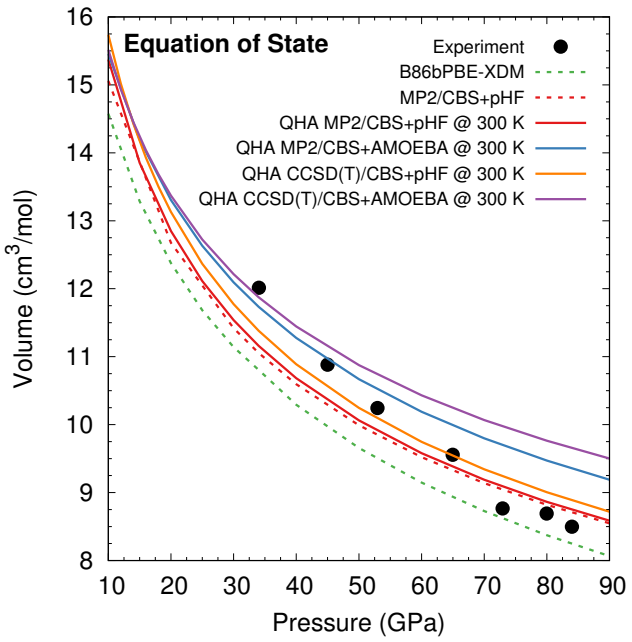

FIG. 4: Comparison of the predicted and experimentally observed[1] equations of state for λ N_2.

perimentally reported structure at 34 GPa and the enthalpic stability of the $P2_1/c$ structure relative to other candidate structures generated by AIRSS crystal structure prediction support the assignment of this structure to the λ phase.

Spectroscopic comparisons: Further insight into this phase is gained by looking at the how the structure and Raman spectrum changes with pressure. Figure 4 plots the equation of state predictions for several different models against experimentally reported volumes. None of the models quite reproduce the experimental volume data. B86bPBE-XDM underestimates the molar volume throughout the pressure range. The QHA MP2 and CCSD(T) results with AMOEBA many-body terms predict consistently larger molar volumes, which end up being closer to the experimental values near ∼30–40 GPa. The molar volumes from the models with periodic HF many-body treatments are consistently smaller and agree better with experiment at higher pressures (as one might expect from the better HF treatment of many-body exchange-overlap at high pressures). For a given many-body treatment, CCSD(T) predicts a slightly larger volume than MP2. The additional expansion obtained by including the QHA treatment is small throughout the pressure range. The impact of the QHA approximation would be more noticeable at even lower pressures, of course.

Using the 300 K QHA CCSD(T) structures, MP2/aug-cc-pVDZ + AMOEBA harmonic phonons and Raman intensities were computed at various pressures. As described in the Methods section, the atomic positions were relaxed within the fixed QHA CCSD(T) unit cells at this same level of theory to ensure stationarity of the energy with respect to atomic position, as required by the harmonic phonon approximation. Figure 5a plots representative spectra at 70 GPa, while Figure 5b predicts how the Raman-active librational mode frequencies vary with pressure. The librational modes provide a useful fingerprint for crystal packing. The number of Raman active modes and their relative intensities in the predicted spectra agree well with the experimental ones. The agreement between the predicted and experimental frequencies is rather good at low pressures, but the errors reach up to ∼50–100 cm^{-1} at high pressures.

While the overall agreement between theory and experiment in the pressure-volume and Raman data is fairly good, it is unclear why the disagreement between the models and experiment is as large as it is. Earlier work on high-pressure phases of carbon dioxide in the ∼10–60 GPa range found that a very similar fragment-based modeling approach generally reproduced the molar volumes to within 1%, while the positions of the Raman-active librational modes were reproduced to within 10–15 cm^{-1}.[10] The treatment of one- and two-body interactions at the CCSD(T)/CBS level is likely well converged (it differs only modestly from the MP2/CBS results). The treatment of the many-body effects appears to be a larger problem, and perhaps computing those contributions with a larger basis set and/or higher level of theory would be helpful. It's possible, for example, that terms such as the generally repulsive Axilrod-Teller-Muto three-body dispersion term or other, higher-order exchange overlap contributions that are missing from HF become important at these high pressures. Alternatively, given the small size and low-orientational specificity of the intermolecular interactions in the crystals, anharmonic and/or dynamical contributions may be more important in high-pressure nitrogen phases than in carbon dioxide.

Beyond possible errors in the modeling, problems with the experimental measurements and their interpretation cannot be ruled out. Pressure gradients, inhomogeneous samples (e.g. due to partial phase transformations), and other factors can impact high-pressure studies such as those used to characterize this phase. Despite the moderate disagreements between theory and experiment, the overall collection of crystal structure and property predictions here support assignment of this $P2_1/c$ structure to the λ phase of nitrogen.

Thermodynamic stability: Finally, we turn to the question of the thermodynamic stability of the λ phase compared to other potential phases it overlaps with on the phase diagram. The original experimental study indicated that the λ phase potentially coexists with nine other phases on the phase diagram: γ, ϵ, ζ, ι, θ, κ, η, cg, and the layered polymeric phase.[1] The fragment-based approach used here is not well-suited to model the network covalent phases, so the cg and layered polymeric phases are not considered further. Those network co-

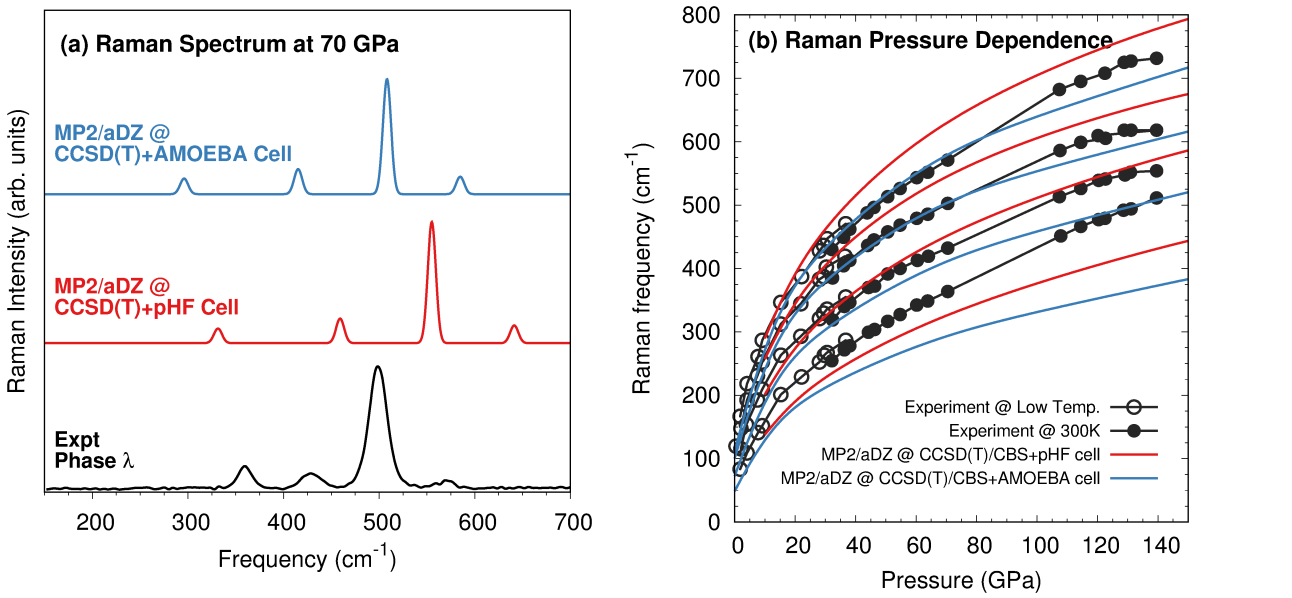

FIG. 5: Comparison of the predicted and experimentally observed[1] Raman spectra for λ nitrogen in the librational region.

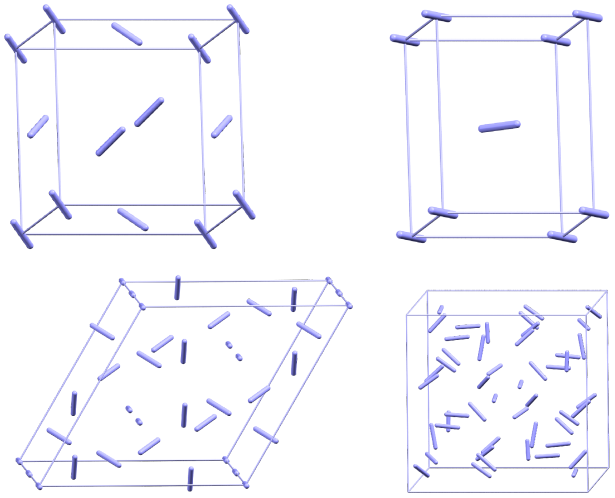

FIG. 6: Crystal structures of N_2 (top left) phase α[58] (top right) phase γ[59] (bottom left) phase ϵ[60] (bottom right) phase ι[7]

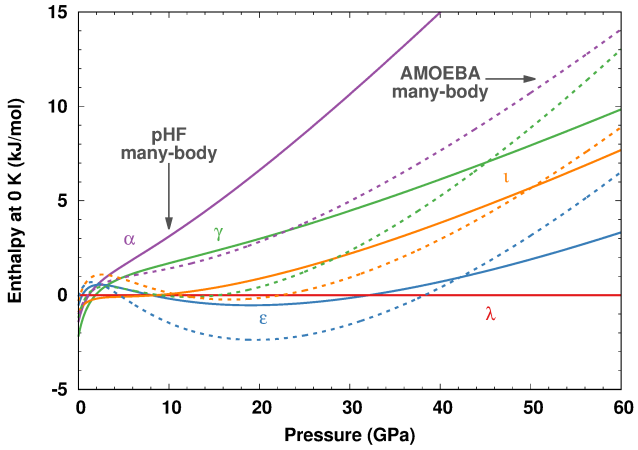

FIG. 7: Comparison of CCSD(T) enthalpies at 0 K for the α, γ, ϵ, λ, and ι phases as a function of pressure using either periodic HF (solid lines) or AMOEBA (dotted lines) for the many-body treatment.

valent nitrogen phases are not likely viable until higher pressures anyways (at least 50 GPa, if not above 100 GPa[5,61,62]). Similarly, the κ and η phases only occur at much higher pressures (above 60 GPa). The ζ and θ phases can be quenched to around ~30 GPa where λ occurs, but modeling of their stabilities is not possible because their structures are currently unknown. Therefore, we focus on the molecular α, γ, ϵ, and ι phases, which are present in the relevant pressure regime (Figure 1) and have known structures (Figure 6).

These other crystal structures were modeled using the same techniques as those used above: the structures were optimized at under various external pressures using B86bPBE-XDM. Single-point energy refinements were performed with fragment-based CCSD(T) calculations, and the optimal 0 K enthalpies determined at each pressure (including Γ-point harmonic vibrational contributions). Figure 7 plots the relative stabilities of the four phases with both periodic HF and AMOEBA many-body contributions.

Experimentally, the low-pressure α phase is most stable until 0.36 GPa.[63] As pressure increases, experiments indicate that γ nitrogen becomes the preferred phase until ~2 GPa,[64,65] at which point it transforms to the ϵ phase. Earlier fully periodic MP2 calculations repro-

duced this behavior nicely, predicting these transitions to occur at 0.42 and 2.25 GPa, respectively.[11] Here, the CCSD(T)/CBS + AMOEBA fragment-based enthalpies at 0 K predict the $\alpha \longrightarrow \gamma$ and $\gamma \longrightarrow \epsilon$ transitions to occur at 0.45 and 3.0 GPa, respectively, which is also in rather good agreement with the experimentally reported transitions. Switching to the pHF many-body treatment stabilizes the γ phase relative to α and ϵ somewhat. The γ-ϵ transition shifts only slightly, to 3.2 GPa, but the α phase (incorrectly) becomes less stable than γ all the way down to zero pressure (by 0.8 kJ/mol). The AMOEBA many-body treatment is nominally performing better than periodic HF for these transitions, though given the subtle differences in energetics between models, this could also represent fortuitous error cancellation. The calculations here also predict the ι phase to be less stable than ϵ in the ∼10–60 GPa range, especially with the periodic HF many-body treatment. This result contrasts earlier PBE DFT calculations,[7] which found ι to be more stable than ϵ. In both cases, however, the energy differences between the two phases are only a few kJ/mol or less, and the calculations are performed at 0 K, rather than the elevated temperatures where ι nitrogen has been observed experimentally.

Regarding the λ phase, both sets of CCSD(T) calculations in Figure 7 suggest that λ may be more stable than the α, γ, ϵ, and ι phases under certain pressure conditions, though the specific pressure windows varies with the many-body treatment. While the uncertainties in the models and the omission of several other phases with unknown or network covalent structures prevent definitive statements, it appears plausible that λ nitrogen may represent a thermodynamically stable phase on the phase diagram, at least at low temperatures.

IV. CONCLUSIONS

To summarize, the experimentally reported crystal structure for λ nitrogen reflected a mixture of partial solution powder x-ray diffraction data together with a previously predicted structure which had similar lattice parameters. Here, a detailed study of λ nitrogen has been carried out to confirm this structure, using both dispersion-corrected density functional theory and higher-level fragment-based MP2 and CCSD(T) calculations. AIRSS crystal structure prediction over monoclinic space groups predicted this λ structure as the most stable monoclinic one by ∼5 kJ/mol or more at 34 GPa. While the lattice constants predicted by B86bPBE-XDM were already in decent agreement with experiment, refining the structure further with MP2 and CCSD(T) brought them even closer to the experimental one. Further support for assigning this structure to the λ phase was provided by comparison between the predicted and experimentally reported equation of state and Raman spectra over a broad pressure range. Taken together, the body of evidence provides support for the λ nitrogen structure first proposed by Frost et al.[1]

Because it has been unclear whether λ nitrogen is the thermodynamically stable or only a kinetically accessible phase under the conditions where it has been observed, the stability of this λ phase relative to that of several other experimental phases which are known to co-exist in the same temperature and pressure conditions was compared. Though the sensitivity/uncertainties associated with energetics are relatively large and not all possible phases have been considered, the results do suggest that the λ phase may well be the thermodynamically most stable phase at low temperatures and moderate pressures.

Finally, on the methodological side, the fragment-based MP2 and CCSD(T) models do generally outperform the B86bPBE-XDM density functional for these nitrogen phases. However, the predicted structures and properties at high pressure are somewhat sensitive to the treatment of many-body interactions. For pressures near ∼100 GPa and above in particular (e.g. where the largest errors in the predicted Raman data occur), it may be important in the future to employ even better treatments of the many-body interactions. Periodic local MP2 corrected with coupled cluster calculations have been demonstrated, for example.[66] Pragmatic approaches that account for many-body dispersion effects might also prove useful.[67,68] More careful assessment of these issues should be carried out in the future.

Acknowledgments

Funding for this work from the National Science Foundation (CHE-1665212) and supercomputer time from XSEDE (TG-CHE110064) are gratefully acknowledged.

* Electronic address: gregory.beran@ucr.edu

[1] M. Frost, R. T. Howie, P. Dalladay-Simpson, A. F. Goncharov, and E. Gregoryanz, Phys. Rev. B **93**, 024113 (2016).
[2] A. F. Goncharov, E. Gregoryanz, H.-K. Mao, and R. J. Hemley, Low Temp. Phys. **27**, 866 (2001).
[3] M. I. Eremets, A. G. Gavriliuk, N. R. Serebryanaya, I. A. Trojan, D. A. Dzivenko, R. Boehler, H. K. Mao, and R. J. Hemley, J. Chem. Phys. **121**, 11296 (2004).
[4] E. Gregoryanz, C. Sanloup, R. Bini, J. Kreutz, H. J. Jodl, M. Somayazulu, H.-K. Mao, and R. J. Hemley, J. Chem. Phys. **124**, 116102 (2006).
[5] E. Gregoryanz, A. F. Goncharov, C. Sanloup, M. Somayazulu, H.-k. Mao, and R. J. Hemley, J. Chem. Phys. **126**, 184505 (2007).
[6] E. Gregoryanz, A. F. Goncharov, R. J. Hemley, H.-k. Mao, M. Somayazulu, and G. Shen, Phys. Rev. B **66**, 224108 (2002).

[7] R. Turnbull, M. Hanfland, J. Binns, M. Martinez-Canales, M. Frost, M. Marqués, R. T. Howie, and E. Gregoryanz, Nature Commun. **9**, 4717 (2018).

[8] C. J. Pickard and R. J. Needs, Phys. Rev. Lett. **102**, 125702 (2009).

[9] K. Aoki, H. Yamawaki, M. Sakashita, Y. Gotoh, and K. Takemura, Science **263**, 356 (1994).

[10] W. Sontising, Y. N. Heit, J. L. McKinley, and G. J. O. Beran, Chem. Sci. **8**, 7374 (2017).

[11] A. Erba, L. Maschio, S. Salustro, and S. Casassa, J. Chem. Phys. **134**, 074502 (2011).

[12] A. Erba, L. Maschio, C. Pisani, and S. Casassa, Phys. Rev. B **84**, 012101 (2011).

[13] M. S. Gordon, D. G. Fedorov, S. R. Pruitt, and L. Slipchenko, Chem. Rev. **112**, 632 (2012).

[14] M. A. Collins and R. P. A. Bettens, Chem. Rev. **115**, 5067 (2015).

[15] K. Raghavachari and A. Saha, Chem. Rev. **115**, 5643 (2015).

[16] G. J. O. Beran, Chem. Rev. **116**, 5567 (2016).

[17] G. J. O. Beran, J. Chem. Phys. **130**, 164115 (2009).

[18] G. J. O. Beran and K. Nanda, J. Phys. Chem. Lett. **1**, 3480 (2010).

[19] G. J. O. Beran, J. D. Hartman, and Y. N. Heit, Acc. Chem. Res. **49**, 2501 (2016).

[20] Y. N. Heit, K. D. Nanda, and G. J. O. Beran, Chem. Sci. **7**, 246 (2016).

[21] Y. N. Heit and G. J. O. Beran, Acta Cryst. B **72**, 514 (2016).

[22] J. L. McKinley and G. J. O. Beran, Faraday Disc. **211**, 181 (2018).

[23] C. Červinka and G. J. O. Beran, Chem. Sci. **9**, 4622 (2018).

[24] C. Červinka and G. J. O. Beran, Phys. Chem. Chem. Phys. **19**, 29940 (2017).

[25] S. Wen and G. J. O. Beran, Cryst. Growth Des. **12**, 2169 (2012).

[26] S. Wen and G. J. O. Beran, J. Chem. Theory Comput. **8**, 2698 (2012).

[27] S. Hirata, K. Gilliard, X. He, J. Li, and O. Sode, Acc. Chem. Res. **47**, 2721 (2014).

[28] S. Hirata, J. Chem. Phys. **129**, 204104 (2008).

[29] O. Sode, M. Keçeli, S. Hirata, and K. Yagi, Int. J. Quant. Chem. **109**, 1928 (2009).

[30] O. Sode and S. Hirata, Phys. Chem. Chem. Phys. **14**, 7765 (2012).

[31] J. Li, O. Sode, G. A. Voth, and S. Hirata, Nature Commun. **4**, 2647 (2013).

[32] O. Sode, M. Keceli, K. Yagi, and S. Hirata, J. Chem. Phys. **138**, 074501 (2013).

[33] J. Li, O. Sode, and S. Hirata, J. Chem. Theory Comput. **11**, 224 (2015).

[34] Y. Han, J. Liu, L. Huang, X. He, and J. Li, npj Quantum Materials **4**, 10 (2019).

[35] X. He, O. Sode, S. S. Xantheas, and S. Hirata, J. Chem. Phys. **137**, 204505 (2012).

[36] K. Gilliard, O. Sode, and S. Hirata, J. Chem. Phys. **140**, 174507 (2014).

[37] M. A. Salim, S. Y. Willow, and S. Hirata, J. Chem. Phys. **144**, 204503 (2016).

[38] A. D. Becke, J. Chem. Phys. **38**, 7184 (1986).

[39] J. P. Perdew, K. Burke, and M. Ernzerhof, Phys. Rev. Lett. **77**, 3865 (1996).

[40] A. Otero-de-la Roza and E. R. Johnson, J. Chem. Phys. **136**, 174109 (2012).

[41] P. Giannozzi, S. Baroni, N. Bonini, M. Calandra, R. Car, C. Cavazzoni, D. Ceresoli, G. L. Chiarotti, M. Cococcioni, I. Dabo, A. Dal Corso, S. de Gironcoli, S. Fabris, G. Fratesi, R. Gebauer, U. Gerstmann, C. Gougoussis, A. Kokalj, M. Lazzeri, L. Martin-Samos, N. Marzari, F. Mauri, R. Mazzarello, S. Paolini, A. Pasquarello, L. Paulatto, C. Sbraccia, S. Scandolo, G. Sclauzero, A. P. Seitsonen, A. Smogunov, P. Umari, and R. M. Wentzcovitch, J. Phys. Condens. Mat. **21**, 395502 (2009).

[42] P. Giannozzi, O. Andreussi, T. Brumme, O. Bunau, M. Buongiorno Nardelli, M. Calandra, R. Car, C. Cavazzoni, D. Ceresoli, M. Cococcioni, N. Colonna, I. Carnimeo, A. Dal Corso, S. de Gironcoli, P. Delugas, R. A. DiStasio, A. Ferretti, A. Floris, G. Fratesi, G. Fugallo, R. Gebauer, U. Gerstmann, F. Giustino, T. Gorni, J. Jia, M. Kawamura, H.-Y. Ko, A. Kokalj, E. Küçükbenli, M. Lazzeri, M. Marsili, N. Marzari, F. Mauri, N. L. Nguyen, H.-V. Nguyen, A. Otero-de-la Roza, L. Paulatto, S. Poncé, D. Rocca, R. Sabatini, B. Santra, M. Schlipf, A. P. Seitsonen, A. Smogunov, I. Timrov, T. Thonhauser, P. Umari, N. Vast, X. Wu, and S. Baroni, J. Phys. Condens. Mat. **29**, 465901 (2017).

[43] P. Ren, C. Wu, and J. W. Ponder, J. Chem. Theory Comput. **7**, 3143 (2011).

[44] Y. Heit and G. J. O. Beran, J. Comp. Chem. **35**, 2205 (2014).

[45] MOLPRO, version 2012.1, a package of ab initio programs, H.-J. Werner, P. J. Knowles, G. Knizia, F. R. Manby, M. Schütz, P. Celani, T. Korona, R. Lindh, A. Mitrushenkov, G. Rauhut, K. R. Shamasundar, T. B. Adler, R. D. Amos, A. Bernhardsson, A. Berning, D. L. Cooper, M. J. O. Deegan, A. J. Dobbyn, F. Eckert, E. Goll, C. Hampel, A. Hesselmann, G. Hetzer, T. Hrenar, G. Jansen, C. Köppl, Y. Liu, A. W. Lloyd, R. A. Mata, A. J. May, S. J. McNicholas, W. Meyer, M. E. Mura, A. Nicklass, D. P. O'Neill, P. Palmieri, D. Peng, K. Pflüger, R. Pitzer, M. Reiher, T. Shiozaki, H. Stoll, A. J. Stone, R. Tarroni, T. Thorsteinsson, and M. Wang, see http://www.molpro.net.

[46] R. M. Parrish, L. A. Burns, D. G. A. Smith, A. C. Simmonett, A. E. DePrince, E. G. Hohenstein, U. Bozkaya, A. Y. Sokolov, R. Di Remigio, R. M. Richard, J. F. Gonthier, A. M. James, H. R. McAlexander, A. Kumar, M. Saitow, X. Wang, B. P. Pritchard, P. Verma, H. F. Schaefer, K. Patkowski, R. A. King, E. F. Valeev, F. A. Evangelista, J. M. Turney, T. D. Crawford, and C. D. Sherrill, J. Chem. Theory Comput. **13**, 3185 (2017).

[47] R. Dovesi, A. Erba, R. Orlando, C. M. Zicovich-Wilson, B. Civalleri, L. Maschio, M. Rérat, S. Casassa, J. Baima, S. Salustro, and B. Kirtman, WIREs Comput. Mol. Sci. **8**, e1360 (2018).

[48] J. W. Ponder, TINKER v6.3, 2014, `http://dasher.wustl.edu/tinker/`, accessed August 10, 2015.

[49] T. Helgaker, W. Klopper, H. Koch, and J. Noga, J. Chem. Phys. **106**, 9639 (1997).

[50] M. F. Peintinger, D. V. Oliveira, and T. Bredow, J. Comp. Chem. **34**, 451 (2013).

[51] F. Weigend and R. Ahlrichs, Phys. Chem. Chem. Phys. **7**, 3297 (2005).

[52] C. F. Macrae, I. J. Bruno, J. A. Chisholm, P. R. Edgington, P. McCabe, E. Pidcock, L. Rodriguez-Monge, R. Taylor, J. van de Streek, and P. A. Wood, J. Appl. Cryst. **41**, 455 (2008).

[53] M. J. Frisch *et al.*, Gaussian 09 Revision E.01, 2009, gaus-

sian Inc. Wallingford CT.
[54] C. J. Pickard and R. J. Needs, J. Phys. Condens. Mat. **23**, 053201 (2011).
[55] A. J. Cruz-Cabeza, S. M. Reutzel-Edens, and J. Bernstein, Chem. Soc. Rev. **44**, 8619 (2015).
[56] J. Nyman and G. M. Day, CrystEngComm **17**, 5154 (2015).
[57] J. A. Chisholm and W. D. S. Motherwell, J. Appl. Crystall. **38**, 228 (2005).
[58] R. W. G. Wyckoff, *Crystal Structures, Volume 1* (Interscience Publishers, New York, New York, 1963).
[59] A. F. Schuch and R. L. Mills, J. Chem. Phys. **52**, 6000 (1970).
[60] R. L. Mills, B. Olinger, and D. T. Cromer, J. Chem. Phys. **84**, 2837 (1986).
[61] A. K. McMahan and R. LeSar, Phys. Rev. Lett. **54**, 1929 (1985).
[62] C. Mailhiot, L. H. Yang, and A. K. McMahan, Phys. Rev. B **46**, 14419 (1992).
[63] C. A. Swenson, J. Chem. Phys. **23**, 1963 (1955).
[64] S. Buchsbaum, R. L. Mills, and D. Schiferl, J. Phys. Chem. **88**, 2522 (1984).
[65] D. Schiferl, S. Buchsbaum, and R. L. Mills, J. Phys. Chem. **89**, 2324 (1985).
[66] C. Müller and D. Usvyat, J. Chem. Theory Comput. **9**, 5590 (2013).
[67] J. Hoja, A. M. Reilly, and A. Tkatchenko, WIREs Comput. Mol. Sci. **7**, e1294 (2017).
[68] Y. Huang and G. J. O. Beran, J. Chem. Phys. **143**, 044113 (2015).